A Simple and Effective Method to Estimate the Model Parameters of Dielectric Barrier Discharge Ozone Chamber

Muhammad Amjad, Zainal Salam, Mochammad Facta, and Kashif Ishaque

***Abstract*—This paper presents a simple yet effective method to determine the electrical model parameters of the dielectric barrier discharge (DBD) ozone chamber at frequencies above 20 kHz. The method is an alternative to the conventional Lissajous plot estimation method which appears to yield unsatisfactory results in this frequency range. Furthermore, the proposed technique allows for the chamber parameters to be determined at different frequencies — a flexibility which is not easily achievable using the typical Lissajous method. The measurement setup consists of a full-bridge inverter and a high-frequency variable inductor connected to the DBD chamber. The inductor can be adjusted to allow for parameter determination at different frequencies. The chamber parameters obtained from experimental results are validated by applying them in a high-voltage power supply for ozone generator.**

***Index Terms*—Electrical modeling, full-bridge inverter, high-frequency variable inductor, ozone chamber, resonant frequency.**

I. Introduction

OZONE GAS is considered as one of the strongest oxidizing agent, yet it leaves no residues that are harmful to global environment. It is easily soluble in water and is used as a substitute of chlorine for the purification of drinking water. Currently, it is applied in many important sectors such as agriculture, water supply, solid waste treatment, and pharmaceutical industries. In agriculture, ozonated water is used for hydroponic applications and for the postharvest treatment of crops. It is known that the shelf life of fruits and vegetables can be increased using ozone gas in cold storages. In water treatment plants, waste water is recycled using ozone gas and disinfection in pipeline systems. In hospitals, it is used as a disinfectant for surgical equipment, clothes, and linens [1]–[3].

Manuscript received May 29, 2011; revised September 13, 2011; accepted October 27, 2011. Date of publication March 8, 2012; date of current version May 11, 2012. The Associate Editor coordinating the review process for this paper was Dr. Thomas Lipe.

M. Amjad is with the Universiti Teknologi Malaysia, Johor Bahru, 81310 Malaysia, and also with the University College of Engineering and Technology, The Islamia University of Bahawalpur, Bahawalpur, 63100 Pakistan (e-mail: Muhammad.Amjad@iub.edu.pk).

Z. Salam is with the Faculty of Electrical Engineering, Universiti Teknologi Malaysia, Johor Bahru, 81310 Malaysia (Corresponding author e-mail: zainals@fke.utm.my).

M. Facta is with the Universiti Teknologi Malaysia, Johor Bahru, 81310 Malaysia (e-mail: mochfacta@gmail.com).

K. Ishaque is with the Universiti Teknologi Malaysia, Johor Bahru, 81310 Malaysia (e-mail: kashif.ishaque@pafkiet.edu.pk).

Color versions of one or more of the figures in this paper are available online at http://ieeexplore.ieee.org.

Digital Object Identifier 10.1109/TIM.2012.2188351

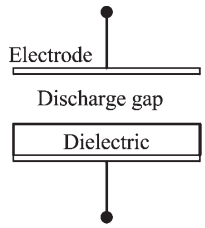

Fig. 1. Basic configuration of a DBD chamber.

Dielectric barrier discharge (DBD) is one of the most efficient method to produce ozone [4]. The basic configuration of DBD chamber for ozone generation is shown in Fig. 1. It consists of two parallel plates (electrodes), one of which is covered with dielectric sheet. Air or oxygen gas is forced to flow in-between a space between the electrodes known as the discharge gap. When high ac voltage is applied between the electrodes, an electric field produces the phenomenon known as DBD [5]–[7]. These discharges cause the bombardment of electrons on oxygen molecules, breaking it to a single O atom inside the discharge gap. This atom combines with O_2 to form ozone gas.

Traditionally, a DBD power supply consists of a high-frequency resonant inverter and a high-voltage transformer. The power supply is operated at a frequency near the resonance to obtain maximum gain. In general, the equivalent electrical parameters are modeled by its impedance and sources, i.e., capacitors (C_a and C_g), resistor (R_p), a diode bridge, and a dc voltage source. The values of these components depend on the width of the discharge gap, dielectric and electrode material, gas flow rate, pressure, and chamber dimensions. Furthermore, the chamber impedance changes with the amount of discharge that occurs between the electrodes. The power supply is designed based on the required power, maximum voltage, and current drawn by the ozone chamber. It is necessary to match the impedance of the chamber with the power supply to transfer maximum power at a specific frequency [8], [9]. Due to this reason, it is important to determine the parameters of the chamber accurately. Hence, modeling is mandatory.

One example of a DBD chamber model is proposed in [10]. Capacitors $C_{\rm gas}$ and $C_{\rm sd}$ are the equivalent capacitances of gas present in the chamber and dielectric, respectively, while $Z_{\rm gas}$ models the variation of gas conductivity during low ionization level. The main disadvantage of this model is that the electrodes' equivalent circuit is not included, and therefore, the power consumption of the chamber could not be estimated.

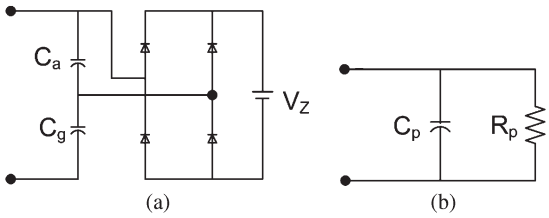

Fig. 2. Model of the ozone chamber. (a) Nonlinear model. (b) Linear model.

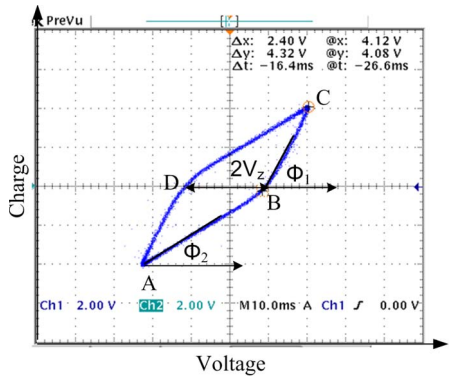

Fig. 3. Experimental measurement of the voltage–charge Lissajous figure of the ozone chamber.

In [11] and [12], a nonlinear model based on diode bridge circuit, shown in Fig. 2(a), is proposed. C_a and C_g are the capacitances due to discharge gap and the dielectric sheet, respectively. The voltage source (V_z) represents the voltage at which the DBD is initiated; when the applied voltage across C_a is greater than V_z, the diode bridge conducts, and the effect of C_a disappears. This implies that the characteristic of the model is nonlinear. However, this model does not consider the losses in the electrodes and is only accurate for a frequency up to 10 kHz. In a linear model proposed in [13], the chamber is represented by the parallel combination of resistor and capacitor. This model is shown in Fig. 2(b) and is normally used at higher frequencies (15–20 kHz). Basically, it is the simplification of the nonlinear model shown in Fig. 2(a). The rectifier and discharge voltage in Fig. 2(a) are replaced by an equivalent resistance R_p. The power consumed in the chamber is represented by R_p. The capacitances C_a and C_g are combined to form an equivalent capacitance C_p.

The typical Lissajous plot for the model proposed in [11] is shown in Fig. 3. The chamber parameters are determined by the voltage–charge $(V-Q)$ using the $X-Y$ plot function of the oscilloscope. The slopes Φ_1 and Φ_2 are used to estimate the values of C_a and C_g using the formulas described in [11]. The voltage V_z is calculated by measuring the distance from the center to the cross point of voltage axis. On the other hand, for the model in [13], the values of chamber parameter C_p and R_p are determined by the voltage–current $(V-I)$ and voltage–charge $(V-Q)$, respectively.

Although Lissajous measurement is widely employed, there are several disadvantages inherent for this method. It is known that the shape of Lissajous plots and, hence, parameter values depend on the frequency of the ozone power supply [11], [13]. At frequencies below 10 kHz, the Lissajous shape resembles a

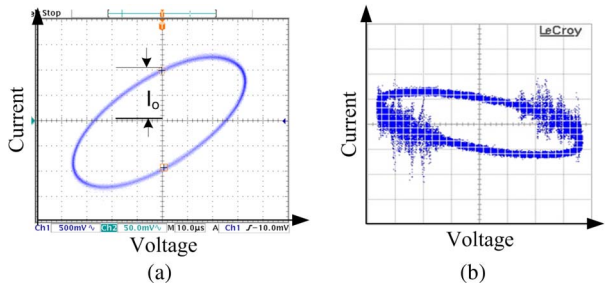

Fig. 4. Experimental measurement of the voltage–current Lissajous figure of the ozone chamber at the frequencies of (a) 15 and (b) 25 kHz.

parallelogram as shown in Fig. 3. Using this plot, the parameters for both the linear and nonlinear models of the chamber can be determined accurately. However, when the frequency is in the 15–20-kHz range, the shape becomes circular; only the linear model parameters can be estimated because the slopes Φ_1 and Φ_2 cannot be determined as shown in Fig 4(a). If the frequency operation is increased beyond 20 kHz, the Lissajous plot becomes irregular with a distorted circular format [14], [15], as shown in Fig. 4(b). Clearly, it is difficult to obtain accurate parameters using this plot.

The typical measurement setup to obtain the chamber parameters consists of a radio frequency (*RF*) amplifier, high-voltage transformer, and an external capacitor connected in series between the chamber and the secondary of the transformer [13], [16]. The frequency of the *RF* amplifier is tuned to be in the vicinity of the resonant frequency. The measurement of the $V-Q$ Lissajous plot is made indirectly across the external capacitor. The frequency of the latter is due to the combination of the chamber parameters and the transformer. Once the *RF* amplifier is tuned to resonance, the power delivered to the chamber can be varied by changing its voltage gain. The parameters, i.e., R_p and C_p, are calculated as a function of the power applied to the chamber. It has to be noted that this setup allows the determination of chamber parameters at only one frequency of operation, i.e., at resonance.

In view of these deficiencies, this paper proposes a simple yet effective method to determine the model parameters of the ozone chamber without utilizing the Lissajous plot. The proposed method is suitable for high-frequency ozone generators (above 20 kHz) where the information extracted from Lissajous figures appear to be unsatisfactory. Furthermore, by utilizing a high-frequency variable inductor, the chamber parameters can be calculated even if the operational frequency is changed—which is not possible by the typical RF amplifier setup mentioned earlier. The proposed measurement setup consists of a full-bridge inverter and a variable high-frequency inductor connected to an ozone chamber. The inductor is connected between the inverter and ozone chamber to form a parallel-loaded resonant circuit. A gate drive circuit is designed to provide stable variable frequency gating signal for the full-bridge inverter. Applying the frequency sweep to the gate drive, the resonant frequency and voltage gain of the parallel-loaded resonant circuit are obtained. Using these information, the chamber parameters are computed mathematically.

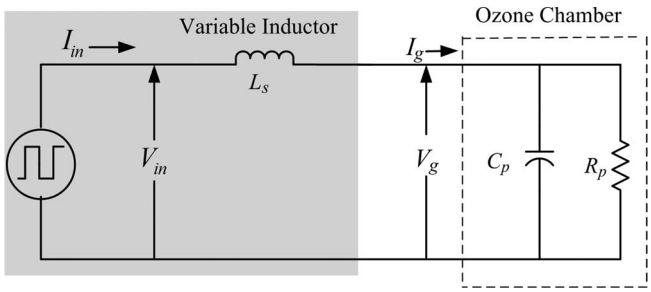

Fig. 5. Circuit diagram of the variable inductor and ozone chamber.

The remaining of this paper is organized as follows: Section II describes the concept of the proposed method and the related analysis. Section III details the measurement setup for the proposed method, while Section IV presents the experimental results. In Section V, the computed ozone chamber parameters are validated by applying them in the design of an ozone generator power supply. Finally, this paper is summarized with a brief conclusion.

II. Principle of the Proposed Method

In the linear model, the ozone chamber is considered as a highly capacitive load [17]. The concept for parameter determination is to integrate the ozone chamber with a variable high-frequency inductor L_s. Consequently, it creates a parallel-loaded resonant circuit, which exhibits a high voltage gain at resonance. Since no external capacitor is added in parallel with the chamber, the voltage gain is proportional to the value of chamber resistance and capacitance only. The resonant frequency of this circuit depends on the external inductor and capacitance of the chamber. Since the input to this circuit is a square wave, the resonant inductor and chamber capacitance also act as a filter; as a result, pure sinusoidal voltage and current waveforms are expected across the chamber. The analysis is made based on the assumption that the fundamental component of the input voltage waveform appears across the chamber. The impedance of the chamber depends upon the frequency of operation; for every value of inductance, there exists a unique value of chamber capacitance at resonant frequency. Fig. 5 shows the equivalent circuit of ozone chamber and external inductor. The input impendence and transfer function of this circuit are given by Cosby and Nelms [18], i.e.,

$$Z_{\text{in}} = \frac{R_p}{1+(\omega R_p C_p)^2} + j\left(\omega L_s - \frac{\omega R_g^2 C_p}{1+\omega R_p^2 C_p^2}\right) \tag{1}$$

$$A_v = \left|\frac{V_o(j\omega)}{V_{\text{in}}(j\omega)}\right| = \frac{1}{\sqrt{\left(1-\left(\frac{\omega}{\omega_p}\right)^2\right)^2 + \left(\frac{\omega}{\omega_p Q_p}\right)^2}} \tag{2}$$

where ω_p is undamped natural frequency given by

$$\omega_p = \frac{1}{\sqrt{L_s C_p}} \tag{3}$$

and Q_p is the loaded quality factor

$$Q_p = \frac{R_p}{\omega_p L_s} = \omega_p C_p R_p. \tag{4}$$

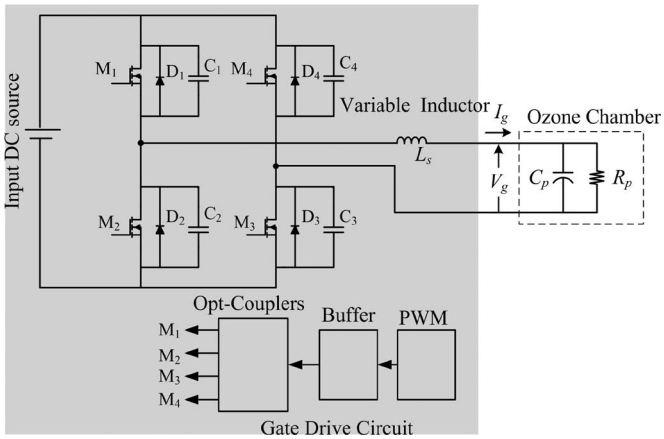

Fig. 6. Measurement setup for ozone chamber parameter determination.

The resonant frequency of the circuit can be found by taking the derivative of (2) with respect to ω, substituting $(d/d\omega)(A_v) = 0$ and $\omega = \omega_r$

$$\omega_r = \omega_p\sqrt{1-\frac{1}{2Q_p^2}} \tag{5}$$

$$A_{\text{vm}} = \frac{Q_p}{\sqrt{1-\frac{1}{4Q_p^2}}}. \tag{6}$$

Note that ω_r is a resonant frequency and A_{vm} is the maximum voltage gain at this frequency. For $Q_p \gg 1$, (5) and (6) can be reduced to

$$\omega_r \cong \omega_p \tag{7}$$

$$A_{\text{vm}} \cong Q_p. \tag{8}$$

The equivalent parallel capacitance C_p can be calculated using (3) and (7), resulting to the following equation:

$$C_p = \frac{1}{\omega_r^2 L_s} \tag{9}$$

where L_s is the known external inductor connected in series with the ozone chamber. The equivalent parallel resistance R_p can be derived using (4) and (8)

$$R_p = A_{\text{vm}}\omega_r L_s. \tag{10}$$

III. Measurement Setup

The measurement setup to calculate ozone chamber parameters is shown in Fig. 6. It consists of a high-frequency full-bridge pulsewidth modulation (PWM) inverter, high-frequency variable inductor, gate drive circuit, and the ozone chamber.

A. PWM Full-Bridge Inverter and Gate Drive Circuit

The full-bridge inverter converts dc voltage into high-frequency square wave voltages. The IRFP460 MOSFET having a freewheeling body diode is used as a switching device. The gate drive circuit is shown in Fig. 7. This circuit provides

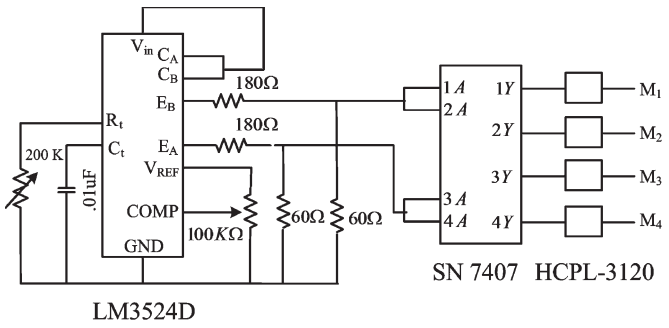

Fig. 7. Gate drive circuit.

the gating signals for MOSFETs $\mathrm{M}_1-\mathrm{M}_4$ in Fig. 6. The gate drive circuit provides stable ac sweep frequency up to 100 kHz. The gate drive signals are generated by regulating the PWM IC LM3524D. The frequency of drive signal is calculated by the voltage-controlled oscillator (VCO). The frequency of VCO is determined by the values of R and C connected at pins R_t and C_t. The outputs of LM3524D are two n-p-n transistors and driven 180° out of phase. Each output of PWM is used to drive two inputs of SN7407 buffer. The duty cycle of the outputs is varied by the voltage applied at the compensation pin of the PWM IC. The four outputs of the buffer are used to drive the four HCPL-3120 optocouplers that provide the gating signal for the inverter.

B. Variable Inductor

The variable high-frequency inductor is designed by area product (A_p) approach [19]. The design parameters are given as the maximum inductance value $L_s = 350$ mH, rated peak current $I_{\mathrm{pk}} = 0.6$ A, and operating frequency $f = 100$ kHz. The value of L_s can be varied from 100 to 350 mH by adjusting the air gap between the cores. The inductor is designed to withstand a maximum voltage of 3 kVp at resonance. It is implemented by putting an isolating tape between the two layers of turns.

The basic expression for the area product is given by

$$A_p = \frac{2(Energy)10^4}{B_m J K_u} \tag{11}$$

$$Energy = \frac{LI_{\mathrm{pk}}^2}{2}. \tag{12}$$

The typical values of the variables are given as follows: operating flux density $B_m = 0.4$ T, current density $J = 250$ A/cm^2, and window utilization factor $K_u = 0.4$. Two inductors are built having each inductance value of 175 mH to implement a 350-mH inductor. From (11), the calculated A_p is 15.75 cm^4. Using the design data of Ferroxcube ferrite core ETD-59, $A_p = 19.0698$ cm^4 and window area $W_a = 5.186$ cm^2. The bare wire area $(A_w(B))$ is calculated as [19]

$$A_w(B) = \frac{I_{\mathrm{rms}}}{J}. \tag{13}$$

The calculated value of $A_w(B)$ is 0.0017 cm^2. From the wire table, the closest value of wire having area to this is $AWG = 24$ $(0.002047$ cm$^2)$. The window effective area $(W_{a(\mathrm{eff})})$ is given by

$$W_{a(\mathrm{eff})} = W_a S_3. \tag{14}$$

The typical value of S_3 is 0.75. The calculated window effective area from (14) is $W_{a(\mathrm{eff})} = 3.8995$ cm^2. The number of turns using insulated wire can be calculated by

$$N = \frac{W_{a(\mathrm{eff})} S_2}{A_w}. \tag{15}$$

With $S_2 = 0.6$, N is calculated to be 931 turns. The photograph of the inductor is shown in Fig. 8.

Fig. 8. Photograph of the high-frequency variable inductor.

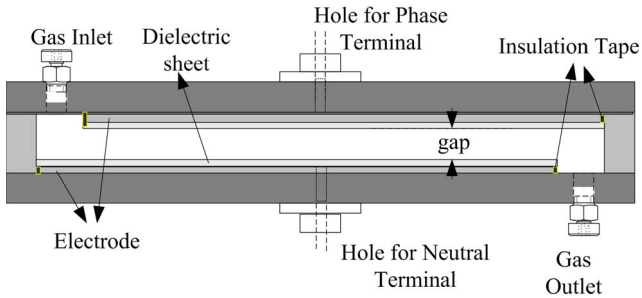

Fig. 9. Ozone chamber configuration.

C. Ozone Chamber

The configuration of the ozone chamber is shown in Fig. 9. The geometry selected consists of parallel electrodes, in which one electrode is covered with dielectric muscovite mica having a 0.1-mm thickness. The dielectric prevents from arc discharge and limits the current flow. The air gap between electrodes is 1 mm. One electrode is made with aluminum wire mesh (outer side covered with Cu tape), and the second electrode is made with copper material. The length of each electrode is 120 mm, and the width is 70 mm.

IV. Experimental Results to Obtain Chamber Parameters

The ozone chamber parameters are obtained using the setup shown in Fig. 6. The voltage and current waveforms are measured using the LeCroy, a 600-MHz digital oscilloscope,

TABLE I
EXPERIMENTAL RESULTS OF THE PARAMETERS OF THE OZONE CHAMBER

Variable Inductance (mH)	Resonance Frequency (KHz)	Voltage Gain (Qp)	Chamber Capacitance (pF)	Chamber Resistance (KΩ)	Chamber Power (W)
336.7	22.8	12.43	145	599.6	1.05
290.6	24.3	12.58	147	558.2	1.09
243.3	26.4	12.24	149.5	508.9	1.10
230	27.1	12.65	150.7	496.1	1.21
193	29.3	12.80	152.5	454.8	1.25
168	31.5	13.00	153	432.3	1.32
145	33.7	13.10	155	402.2	1.36
128	35.4	13.26	157	377.5	1.42
116	37.2	13.47	158	365.2	1.48
95	40.8	13.68	161.5	333.2	1.56

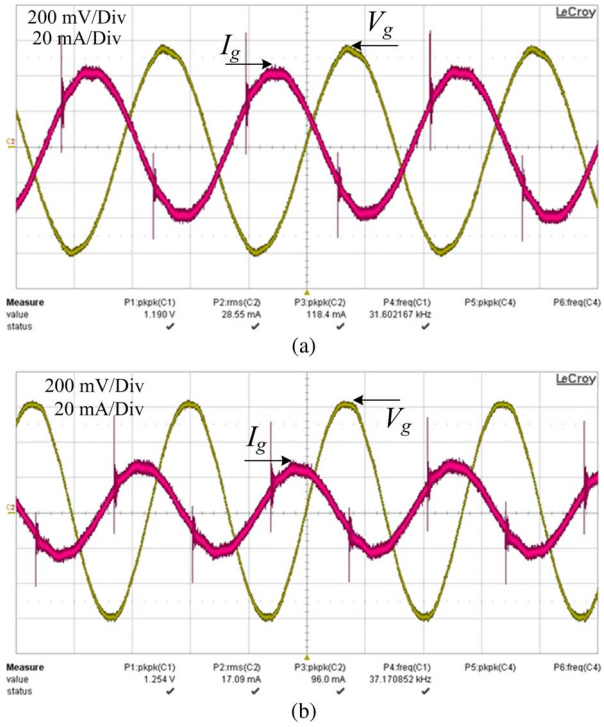

Fig. 10. Voltage and current waveforms of the ozone chamber at various resonant frequencies: At the resonant frequencies of (a) 31.5 and (b) 37.2 kHz.

equipped with high voltage and current probe. The ozone chamber is supplied with normal air at a flow rate of 0.82 L/min. The value of the inductance is varied; as a result, the chamber parameters are calculated at different frequencies. The switching frequency of inverter is varied by slowly sweeping the frequency of the gate drive circuit until resonant frequency is achieved. The resonant frequency and voltage gain are obtained experimentally for each inductance value which is used to determine the parameters C_p and R_p of the ozone chamber.

The inductance is varied from 336.7 to 95 mH, while the input of the inverter is fixed at 35 V. The resonant frequency and voltage gain are measured, and the results are shown in Table I. The chamber capacitance (C_p) and resistance (R_p) are calculated using (9) and (10), respectively.

Fig. 10 shows the current and voltage waveforms of the ozone chamber at different resonant frequencies. The voltage and current waveforms are sinusoidal, hence confirming the operation at resonance. The current waveform of the ozone

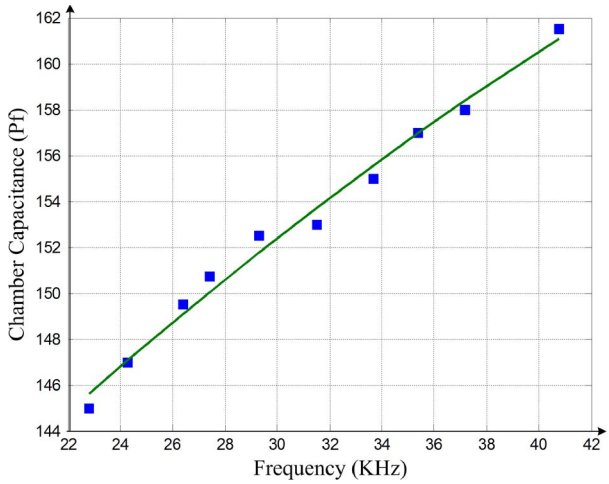

Fig. 11. Variation of chamber equivalent capacitance with frequency.

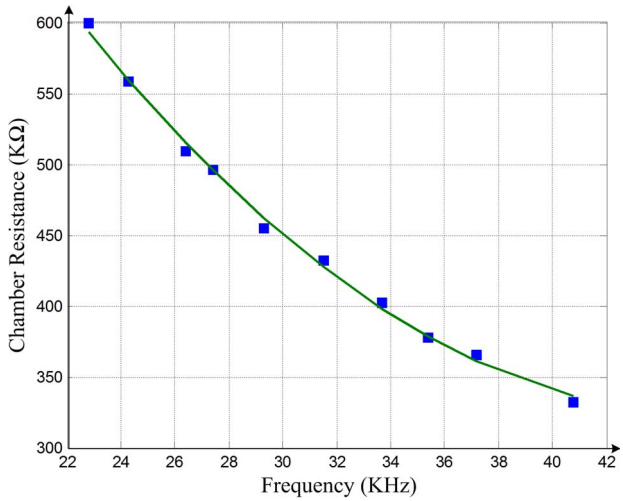

Fig. 12. Variation of ozone chamber resistance with frequency.

chamber during positive and negative cycles contains high-frequency spikes, which indicates the occurrences of discharge in the chamber.

Fig. 11 shows the variation of equivalent chamber capacitance with the frequency of the inverter. By increasing the inverter frequency, the equivalent capacitance and current of the ozone chamber increases; as a result, the power supplied to the chamber increases as indicated in Table I. Fig. 12 shows the equivalent resistance of the ozone chamber. It decreases with increasing the frequency, which is in agreement with the trend in [20]–[22].

V. VALIDATION OF CHAMBER PARAMETERS

To validate the correctness of the proposed method, a high-voltage power supply for an ozone generator is designed [23]. The topology selected is the half-bridge resonant inverter using the parallel LC tank. The chamber parameters obtained from the proposed estimation methods are as follows: resonant frequency 31.5 kHz, $C_p = 153$ pF, and $R_p = 432$ kΩ. The resonant power supply is designed using the following parameters: input voltage $V_{cc} = 50$ V, input power $P_{avg} = 13$ W, and

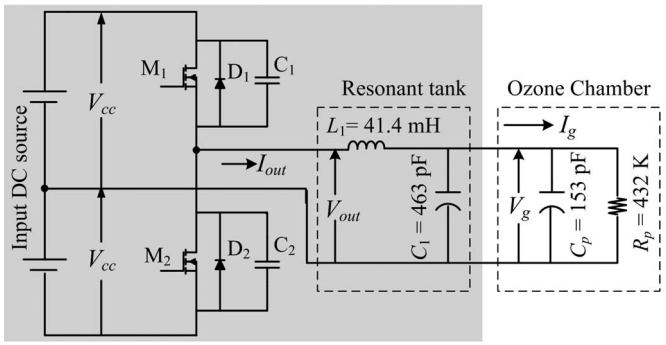

Fig. 13. Experimental setup of the resonant power supply and ozone chamber.

the switching frequency of 31.5 kHz. The circuit diagram of the power supply (shaded) connected to the ozone chamber is shown in Fig. 13. The average power delivered to the chamber can be computed as

$$P_{\text{avg}} = \frac{V_{\text{out,rms}}^2}{R_p}. \tag{16}$$

The maximum voltage gain (A_{vm}) of the chamber at resonance is given by

$$A_{\text{vm}} = \frac{\pi\sqrt{P_{\text{avg}}R_p}}{2\sqrt{2}V_{\text{cc}}}. \tag{17}$$

If the input frequency of the signal to the resonant tank and chamber is equal to the resonant frequency of the circuit; then, the maximum voltage gain, the loaded quality factor (Q_p) of the circuit, can be expressed as

$$Q_p = A_{\text{vm}} = \frac{R_p}{\omega_p L_1} = \omega_p(C_1 + C_p)R_p. \tag{18}$$

The values of L_1 and C_1 can be determined by combining (17) and (18), i.e.,

$$L_1 = \frac{2\sqrt{2}V_{\text{cc}}}{\pi\omega_p}\sqrt{\frac{R_p}{P_{\text{avg}}}} \tag{19}$$

$$C_1 = \frac{\pi}{2\sqrt{2}\omega_p V_{\text{cc}}}\sqrt{\frac{P_{\text{avg}}}{R_p}} - C_p. \tag{20}$$

From (19) and (20), the values of the resonant tank components, i.e., L_1 and C_1, are computed to be 41.4 mH and 463 pF, respectively. The transfer function of the resonant tank and ozone chamber is given by

$$A_V = \frac{V_{\text{out}}(S)}{V_{\text{in}}(s)} = \frac{R_p}{L_1R_p(C_1 + C_p)S^2 + L_1S + R_p}. \tag{21}$$

Using the designed values of L_1 and C_1 and the values of the chamber parameters at 31.5 kHz, the plot of the transfer function is shown in Fig. 14. It can be seen that the maximum gain of 52 is obtained at the expected frequency of 31.5 kHz. The output voltage and current waveforms of the resonant inverter are shown in Fig. 15.

To further validate the accuracy of the proposed method, a comparison is carried out with MATLAB/SIMULINK simulation. The simulation model of the resonant power supply

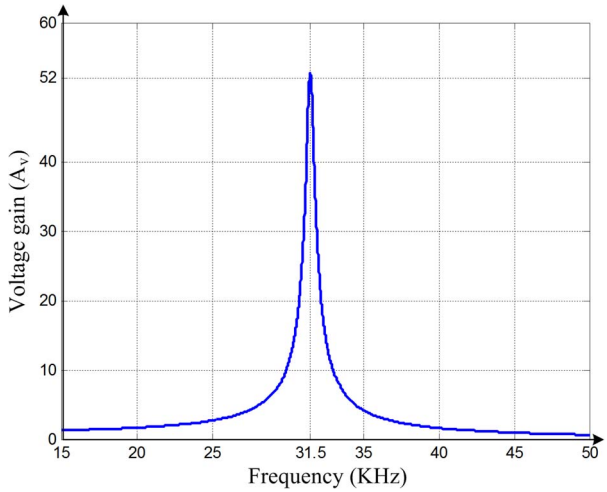

Fig. 14. Voltage gain of the circuit with frequency.

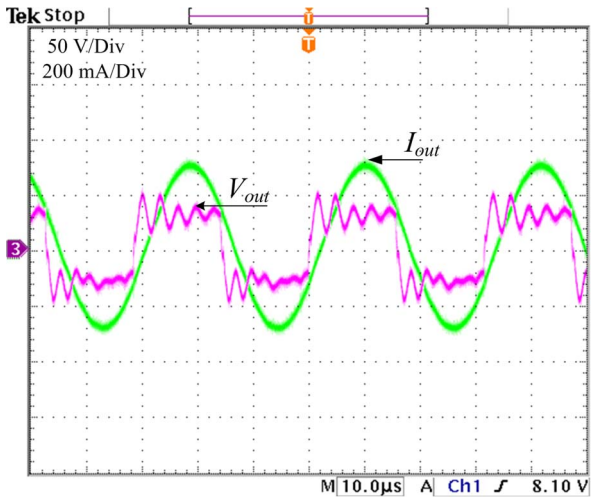

Fig. 15. Inverter output voltage and current.

and chamber is shown in Fig. 16. To be consistent with the experiment, the power supply is designed at a frequency of 31.5 kHz. Fig. 17(a) and (b) show the simulated and experimental waveforms of the chamber, respectively. The experimental resonant frequency (31.8 kHz) is found to be very close to the designed value, thus validating the value of C_p. The experimental peak output voltage of the ozone chamber is also found to be in close agreement with the simulation, which confirms that the value of R_p is acceptable.

The variation of ozone quantity (mgO_3/kWh) with the chamber voltage is shown in Fig. 18. By increasing the applied voltage, discharges from the dielectric barrier will be increased. As a result, the ozone quantity increases in the chamber. However, it has to be noted that the material used as the dielectric, i.e., mica, exhibits a low dielectric strength. Experimental test shows that the chamber can withstand 3.5 kVp–p without experiencing dielectric breakdown. Fig. 19 shows the experimental efficiency of the resonant power supply versus the applied chamber voltage. In general, the efficiency increases with voltage, and the maximum inverter efficiency achieved by the chamber voltage is about 86%. No efficiency measurement is made beyond 3.4 kVp–p due to the limitation in the mica's dielectric strength.

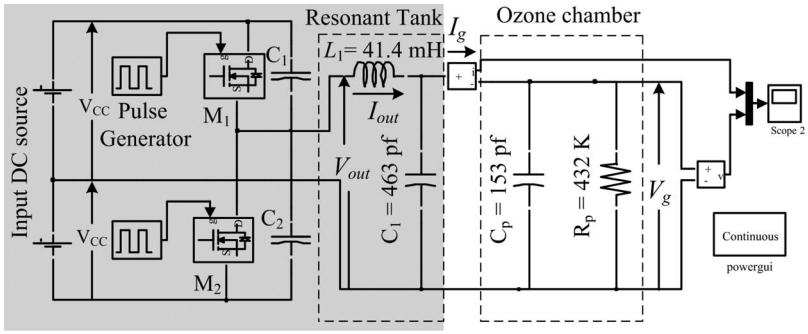

Fig. 16. Power supply and ozone chamber circuit simulation using MATLAB/SIMULINK.

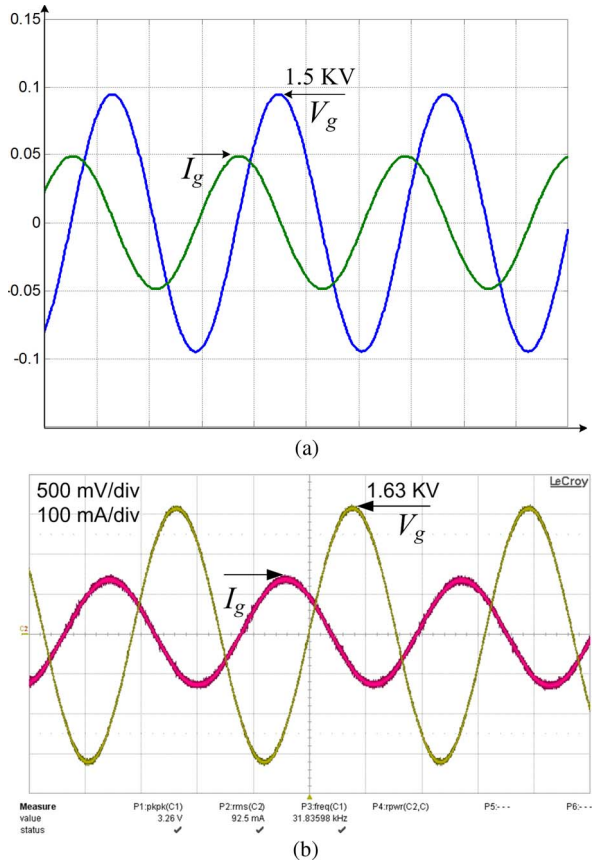

Fig. 17. Voltage and current waveforms of ozone chamber: (a) Simulation and (b) experimental.

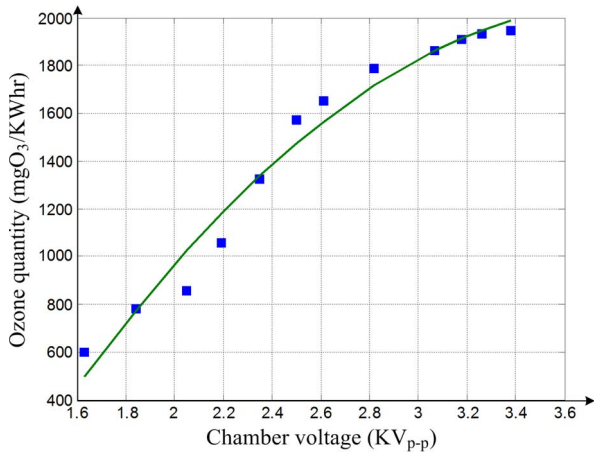

Fig. 18. Variation of ozone quantity with chamber voltage.

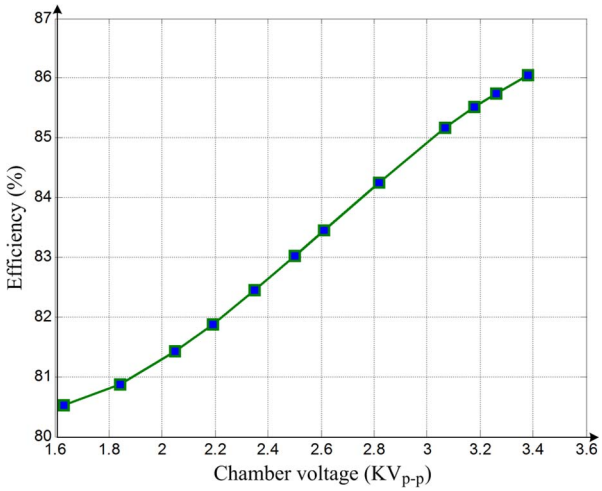

Fig. 19. Efficiency of the resonant power supply with chamber voltage.

VI. Conclusion

In this paper, a simple method to determine the ozone chamber equivalent linear model parameters based on the resonant frequency has been proposed. This method can be specifically used to find the ozone chamber parameters at high frequencies. The analysis and methodology to evaluate the ozone chamber parameters has been presented. The proposed method can be a useful tool to design power supplies at various frequencies. The correctness of the estimated chamber parameters are validated by designing a high-voltage resonant power supply for ozone generator. The simulation and experimental results are found to be in good agreement, which confirms the accuracy of the proposed method.

The contributions of this paper can be summarized as follows.

1) This paper proposes a simple method to determine the model parameters of the ozone chamber without utilizing the Lissajous plots. The method is suitable for parameter estimation at a high frequency (above 20 kHz) when the results obtained using Lissajous plots appear to be unsatisfactory.
2) Another advantage of the proposed method is that the ozone chamber parameter characteristics can be determined for various frequencies without a significant modification of the measurement setup.

ACKNOWLEDGMENT

The authors would like to thank Universiti Teknologi Malaysia for providing the facilities and research grant to conduct this research through Vote No. 79411.

REFERENCES

[1] F. L. Evans, *Ozone in Water and Waste Water Treatment*, 1975.
[2] U. Kogelschatz and B. Eliasson, "Ozone generation and application," in *A Handbook of Electrostatic Processes*. New York: Marcel Dekker, 1995, ch. 26, pp. 581–606.
[3] Z. B. Guzel-Seydim, A. K. Greene, and A. C. Seydim, "Use of ozone in the food industry," *Lebensmittel-Wissenschaft Technol.*, vol. 37, no. 4, pp. 453–460, Jun. 2004.
[4] J. M. Alonso, J. Garcia, A. J. Calleja, J. Ribas, and J. Cardesin, "Analysis, design, and experimentation of a high-voltage power supply for ozone generation based on current-fed parallel-resonant push–pull inverter," *IEEE Trans. Ind. Appl.*, vol. 41, no. 5, pp. 1364–1372, Sep./Oct. 2005.
[5] Z. Falkenstein, "Applications of dielectric barrier discharges," in *Proc. 12th Int. Conf. BEAMS*, 1998, vol. 1, pp. 117–120.
[6] U. Kogelschatz, B. Eliasson, and W. Egli, "Dielectric-barrier discharges: Principle and applications," *J. Phys. IV France*, vol. 7, no. C4, pp. 47–66, 1997.
[7] U. Kogelschatz, "Dielectric-barrier discharges: Their history, discharge physics, and industrial applications," *Plasma Chem. Plasma Process.*, vol. 23, no. 1, pp. 1–46, Mar. 2003.
[8] Y.-X. Cai, W.-D. Zhao, J. Wang, B. Zhou, and W.-H. Han, "Study on optimal matching of DBD load and inverter power of series resonant type," in *Proc. APPEEC*, 2010, pp. 1–4.
[9] Z. Chen and J. R. Roth, "Impedance matching for one atmosphere uniform glow discharge plasma (OAUGDP) reactors," in *Conf. Rec. IEEE Power Plasma Sci.—Abstracts*, 2001, p. 313.
[10] F. Massines, N. Gherardi, N. Naudé, and P. Ségur, "Glow and Townsend dielectric barrier discharge in various atmosphere," *Plasma Phys. Controlled Fusion*, vol. 47, no. 12B, p. B577, Dec. 2005.
[11] O. Koudriavtsev, S. Wang, Y. Konishi, and M. Nakaoka, "A novel pulse-density-modulated high-frequency inverter for silent-discharge-type ozonizer," *IEEE Trans. Ind. Appl.*, vol. 38, no. 2, pp. 369–378, Mar./Apr. 2002.
[12] M. Ponce, J. Aguilar, J. Fernandez, E. Beutelspacher, J. M. Calderon, and C. Cortes, "Linear and non linear models for ozone generators," in *Proc. 9th IEEE Int. CIEP*, 2004, pp. 251–256.
[13] J. M. Alonso, M. Valdés, J. Calleja, J. Ribas, and J. Losada, "High frequency testing and modeling of silent discharge ozone generators," *Ozone: Sci. Eng., J. Int. Ozone Assoc.*, vol. 25, no. 5, pp. 363–376, 2003.
[14] V. H. Olivares, M. Ponce-Silva, R. Osorio, and M. Juarez, "DBD modeling as a function of waveforms slope," in *Proc. IEEE PESC*, 2007, pp. 1417–1422.
[15] V. Kinnares and P. Hothongkham, "Circuit analysis and modeling of a phase-shifted pulsewidth modulation full-bridge-inverter-fed ozone generator with constant applied electrode voltage," *IEEE Trans. Power Electron.*, vol. 25, no. 7, pp. 1739–1752, Jul. 2010.
[16] J. M. Alonso, J. Cardesin, E. L. Corominas, M. Rico-Secades, and J. Garcia, "Low-power high-voltage high-frequency power supply for ozone generation," *IEEE Trans. Ind. Appl.*, vol. 40, no. 2, pp. 414–421, Mar./Apr. 2004.
[17] C. Ordiz, J. M. J. Alonso, M. A. D. Costa, J. Ribas, and A. J. Calleja, "Development of a high-voltage closed-loop power supply for ozone generation," in *Proc. 23rd Annu. IEEE APEC*, 2008, pp. 1861–1867.
[18] M. C. Cosby, Jr. and R. M. Nelms, "A resonant inverter for electronic ballast applications," *IEEE Trans. Ind. Electron.*, vol. 41, no. 4, pp. 418–425, Aug. 1994.
[19] Wm Colonel and T. Mclyman, *Transformer and Inductor Design Handbook*., 3rd ed. New York: Maracel Dekker, 2004.
[20] P. Hothongkham and V. Kinnares, "Measurement of an ozone generator using a phase-shifted PWM full bridge inverter," in *Proc. IPEC*, 2010, pp. 1552–1559.
[21] P. Hothongkham and V. Kinnares, "High-voltage high-frequency power supply using a phase-shifted PWM full bridge inverter fed ozone generator with constant applied electrode voltage," in *Proc. IPEC*, 2010, pp. 1560–1567.
[22] P. Hothongkham and V. Kinnares, "Analysis and modelling of an ozone generator using a phase-shift PWM full bridge inverter," in *Proc. IEEE Int. Conf. ROBIO 2008*, 2009, pp. 1619–1624.
[23] N. Burany, L. Huber, and P. Pejovic, "Corona discharge surface treater without high voltage transformer," *IEEE Trans. Power Electron.*, vol. 23, no. 2, pp. 993–1002, Mar. 2008.

Muhammad Amjad received the B.Sc. and M.Sc. degrees in electrical engineering from the University of Engineering and Technology, Lahore, Pakistan, in 1998 and 2006, respectively. He is currently working toward the Ph.D. degree in electrical engineering at Universiti Teknologi Malaysia, Johor Bahru, Malaysia.

He has been a Lecturer with the University College of Engineering and Technology, The Islamia University of Bahawalpur, Bahawalpur, Pakistan, for ten years. His research interests include the modeling of dielectric barrier discharge (DBD) chamber and power electronic converter for DBD applications.

Zainal Salam received the B.Sc. degree from the University of California, Los Angeles, in 1985, the M.E.E. degree from Universiti Teknologi Malaysia (UTM), Johor Bharu, Malaysia, in 1989, and the Ph.D. degree from the University of Birmingham, Birmingham, U.K., in 1997.

He has been with UTM for 25 years, where he was a Lecturer, is currently a Professor in power electronics with the Faculty of Electrical Engineering, and is also currently the Director with the Inverter Quality Control Center, which is responsible to test Photovolatic inverters that are to be connected to the local utility grid. He has been working in several research studies and consulting works on battery-powered converters, solar energy, and machine control. His research interests include all areas of instrumentation and control in renewable energy.

Mochammad Facta received the B.S. degree in electrical enginering from Universitas Hasanuddin, Makassar, Indonesia, and the M.Eng. degree from Institut Teknologi Sepuluh Nopember, Surabaya, Indonesia. He is currently working toward the Ph.D. degree at Universiti Teknologi Malaysia, Johor Bahru, Malaysia.

He is a Lecturer with Universitas Diponegoro, Semarang, Indonesia.

Kashif Ishaque received the B.E. degree in industrial electronics engineering from the Institute of Industrial Electronics Engineering, Nadirshaw Eduljee Dinshaw University of Engineering and Technology, Karachi, Pakistan, in 2007 and the M.E. degree in mechatronics and automatic control from Universiti Teknologi Malaysia, Johor Bahru, Malaysia, in 2009, where he is currently working toward the Ph.D. degree in electrical engineering.

He is an Assistant Professor with the Pakistan air force Karachi Institute of Economics and Technology, Karachi. His research interests include photovoltaic modeling and control, intelligent control, nonlinear systems control, and optimization techniques such as genetic algorithm, particle swarm optimization, and differential evolution.